# Aalto University

You, Taekho; Kwon, Minji; Jo, Hang-Hyun; Jung, Woo-Sung; Baek, Seung Ki

## Chaos and unpredictability in evolution of cooperation in continuous time

# Chaos and unpredictability in evolution of cooperation in continuous time

Taekho You,[1] Minji Kwon,[1] Hang-Hyun Jo,[2,3,4,*] Woo-Sung Jung,[1,2,3,†] and Seung Ki Baek[5,‡]

[1]*Department of Industrial and Management Engineering, Pohang University of Science and Technology, Pohang 37673, Korea*
[2]*Asia Pacific Center for Theoretical Physics, Pohang 37673, Korea*
[3]*Department of Physics, Pohang University of Science and Technology, Pohang 37673, Korea*
[4]*Department of Computer Science, Aalto University, Espoo FI-00076, Finland*
[5]*Department of Physics, Pukyong National University, Busan 48513, Korea*

Cooperators benefit others with paying costs. Evolution of cooperation crucially depends on the cost-benefit ratio of cooperation, denoted as $c$. In this work, we investigate the infinitely repeated prisoner's dilemma for various values of $c$ with four of the representative memory-one strategies, i.e., unconditional cooperation, unconditional defection, tit-for-tat, and win-stay-lose-shift. We consider replicator dynamics which deterministically describes how the fraction of each strategy evolves over time in an infinite-sized well-mixed population in the presence of implementation error and mutation among the four strategies. Our finding is that this three-dimensional continuous-time dynamics exhibits chaos through a bifurcation sequence similar to that of a logistic map as $c$ varies. If mutation occurs with rate $\mu \ll 1$, the position of the bifurcation sequence on the $c$ axis is numerically found to scale as $\mu^{0.1}$, and such sensitivity to $\mu$ suggests that mutation may have nonperturbative effects on evolutionary paths. It demonstrates how the microscopic randomness of the mutation process can be amplified to macroscopic unpredictability by evolutionary dynamics.

## I. INTRODUCTION

The notion of "evolutionary progress" has been debated ever since Darwin [1], and most evolutionary biologists dismiss the idea that evolution is directional change toward the better [2]. A counterexample to progressionism is self-extinction caused by individual adaptation [3], which is directional change towards the worse by any measure. For example, transgenic males of Japanese medaka fish *Oryzias latipes* have larger body sizes than the wild-type counterparts and thus enjoy advantages in mating, but they tend to decrease the population size because their offspring have lower fecundity [4]. Here, individual interests contradict with the collective interest of the population [5], as is often modeled by the prisoner's dilemma (PD) game. The PD game thus provides us with an analytic model in which selection works in an undesirable direction. However, one could even ask whether evolution is directional after all, and progressionism will lose big ground if chaos proves ubiquitous in evolution, i.e., marking natural history as unpredictable alternations of progression and retrogression. In fact, a recent study indicates that chaos becomes more likely as the dimensionality of the phenotype space increases [6], and the possibility is greatly enhanced by discrete-time dynamics, especially when one considers a wide range of parameters [7]. For example, chaos in the iterated version of the PD game has been reported among 10 different strategies under frequency-dependent selection in discrete time [8]. On the other hand, chaos in low-dimensional continuous dynamics is a more challenging issue, considering that chaos is impossible when the dimensionality of the strategy space is less than three [9]. In this work, we report chaoticity in

three-dimensional (3D) continuous-time mutation-selection dynamics of the iterated PD game with varying the cost-benefit ratio of cooperation. By choosing the PD game as a microscopic foundation, we put our problem into the context of conflict between individual and collective interests in a biological population. In particular, compared with the generic model in Ref. [6], we will see that our approach directly relates unpredictability to mutation, whereas self-extinction can be driven solely by selection, so that it naturally incorporates another key argument of nonprogressionism, i.e., historical contingency of mutation [10].

This work is organized as follows: We explain the basic formulation of our dynamical system in the next section. Section III shows numerical results, which will be discussed in Sec. IV from the viewpoint of time reversal. We will then summarize this work in Sec. V.

## II. METHOD

The PD game is a symmetric two-person game defined by the following payoff table for the row player:

$$\begin{pmatrix} & C & D \\ C & b-c & -c \\ D & b & 0 \end{pmatrix}, \qquad (1)$$

where $C$ and $D$ denote two possible moves, i.e., cooperation and defection, respectively. Note that the payoff table is parametrized by $b$ and $c$ which we assume to satisfy $b > c > 0$. If you choose to cooperate, it implies that it benefits your coplayer by an amount of $b$ at the expense of your own cost $c$. This is the reason that your payoff becomes $-c$ whereas the coplayer earns $+b$ when you cooperate and the coplayer defects [Eq. (1)]. Even if we begin with a group of cooperating individuals, a defecting trait will invade and take over the population as soon as it comes into existence through mutation, which is comparable to the scenario of

*hang-hyun.jo@apctp.org
†wsjung@postech.ac.kr
‡seungki@pknu.ac.kr

self-extinction [3]. The situation changes when the PD game is iterated between the pair of players so that an individual may adopt a strategy according to which cooperation is conditioned on the past interaction with the coplayer. A famous conditional cooperator of this sort is tit-for-tat (TFT), which cooperates at the first round and then copies the coplayer's previous move at each subsequent round [11]. Another important strategy is win-stay-lose-shift (WSLS), which attempts a different move from the previous one if it did not earn a positive payoff [12]. Both TFT and WSLS belong to a class of memory-one strategies in the sense that they refer to only the previous round in making decisions. These conditional cooperators achieve a high level of cooperation based on reciprocity when the cost of cooperation is low enough [13]. Some animal societies seem to have developed such behavior [14]. To contrast those conditional strategies with unconditional ones, we denote a strategy of unconditional cooperation (defection) as AllC (AllD) henceforth. Although the unconditional strategies are memoryless, they are also members of the memory-one strategy class with trivial dependence on the past memory. These are the most extensively studied strategies, so the following strategy set will be considered in this work: $\mathcal{S} \equiv$ {AllC, AllD, TFT, WSLS}.

Let us consider the case when a player with strategy $i \in \mathcal{S}$ plays the iterated PD game against the coplayer with strategy $j \in \mathcal{S}$. At each round, they can occupy one of the following states: $(C,C)$, $(C,D)$, $(D,C)$, and $(D,D)$. Suppose that the result is $(\alpha,\beta)$, or in short $\alpha\beta$, at a current round $(\alpha,\beta \in \{C,D\})$. Based on this result, each player's strategy prescribes cooperation with certain probability, which is either zero or one. The probability that the player (coplayer) with strategy $i$ ($j$) cooperates at the next round is denoted by $q_{\alpha\beta}$ ($r_{\beta\alpha}$). For example, for a player with AllC, $q_{\alpha\beta} = 1$ for all states of $\alpha\beta$, while for a player with TFT, $q_{CC} = q_{DC} = 1$ and $q_{CD} = q_{DD} = 0$ (for details, see Appendix A). The values of $r_{\beta\alpha}$ can be similarly assigned. In the presence of implementation error with probability $\epsilon \in (0,1)$, the probabilities are effectively changed to $q'_{\alpha\beta} = (1 - \epsilon)q_{\alpha\beta} + \epsilon(1 - q_{\alpha\beta})$ and $r'_{\beta\alpha} = (1 - \epsilon)r_{\beta\alpha} + \epsilon(1 - r_{\beta\alpha})$, respectively. By defining $\bar{q}'_{\alpha\beta} \equiv 1 - q'_{\alpha\beta}$ and $\bar{r}'_{\beta\alpha} \equiv 1 - r'_{\beta\alpha}$, the transition matrix between the current and next states is written as

$$M = \begin{bmatrix} q'_{CC}r'_{CC} & q'_{CD}r'_{DC} & q'_{DC}r'_{CD} & q'_{DD}r'_{DD} \\ q'_{CC}\bar{r}'_{CC} & q'_{CD}\bar{r}'_{DC} & q'_{DC}\bar{r}'_{CD} & q'_{DD}\bar{r}'_{DD} \\ \bar{q}'_{CC}r'_{CC} & \bar{q}'_{CD}r'_{DC} & \bar{q}'_{DC}r'_{CD} & \bar{q}'_{DD}r'_{DD} \\ \bar{q}'_{CC}\bar{r}'_{CC} & \bar{q}'_{CD}\bar{r}'_{DC} & \bar{q}'_{DC}\bar{r}'_{CD} & \bar{q}'_{DD}\bar{r}'_{DD} \end{bmatrix}, \quad (2)$$

which admits a unique right eigenvector $\vec{v} = (v_{CC}, v_{CD}, v_{DC}, v_{DD})$ with eigenvalue one according to the Perron-Frobenius theorem. We normalize $\vec{v}$ by requiring $v_{CC} + v_{CD} + v_{DC} + v_{DD} = 1$ to take it as stationary probability distribution over the four states. Note that the existence of error with $\epsilon > 0$ makes the initial state irrelevant in the long run. This procedure is applied to every pair of strategies $i$ and $j$ in $\mathcal{S}$. By taking the inner product between the resulting $\vec{v}$ with a payoff vector $(b - c, -c, b, 0)$, we calculate the long-term payoff $a_{ij}$ that strategy $i$ obtains against $j$ (see Appendix A for details).

Let $x_i(t)$ denote the fraction of strategy $i \in \mathcal{S}$ at time $t$. If the population is infinitely large, $x_i$ can be regarded

as a real variable. The payoff of strategy $i$, denoted by $p_i(t)$, is given as $p_i(t) = \sum_j a_{ij}x_j(t)$ if the population is well mixed. The population average payoff will thus be $\langle p \rangle(t) \equiv \sum_i p_i(t)x_i(t) = \sum_{ij} a_{ij}x_i(t)x_j(t)$. We describe the mutation-selection dynamics of the population using the replicator dynamics (RD) [15,16] as follows:

$$\frac{dx_i}{dt} = f_i \equiv (1 - \mu)p_i x_i - \langle p \rangle x_i + \frac{\mu}{|\mathcal{S}| - 1} \sum_{j \neq i} p_j x_j, \quad (3)$$

where $\mu$ denotes the rate of mutation. We have only three degrees of freedom because $|\mathcal{S}| = 4$ and $\sum_{i \in \mathcal{S}} x_i(t) = 1$ all the time. The system described by Eq. (3) is therefore understood as a deterministic dynamical system inside a 3D region, defined as $\Omega = \{\mathbf{x} \equiv (x_{\text{AllD}}, x_{\text{TFT}}, x_{\text{WSLS}}) | x_{\text{AllD}} \geqslant 0, x_{\text{TFT}} \geqslant 0, x_{\text{WSLS}} \geqslant 0, \text{ and } x_{\text{AllD}} + x_{\text{TFT}} + x_{\text{WSLS}} \leqslant 1\}$. Note that the time scale governing the RD has been assumed to be much larger than that for calculating the "long-term" payoffs. Our main finding is that the dynamics of Eq. (3) exhibits chaos in this $\Omega$ when $\mu > 0$. Our system is minimal to be chaotic, and this minimal system helps us understand the role of mutation in analytic terms.

## III. RESULT

Numerically, we integrate this set of ordinary differential equations for every $i \in \mathcal{S}$ by means of the fourth-order Runge-Kutta method, with enforcing the normalization condition $\sum_{i \in \mathcal{S}} x_i(t) = 1$ at any time $t$. We set $b = 1$ without loss of generality, and take $\epsilon = 10^{-2}$ as the probability of error. We choose $\Delta t = 10^{-2}$ as the incremental time interval for numerical integration throughout this work. Note that the RD depends on the initial condition at $t = 0$ due to its deterministic nature. It is therefore important to probe many different initial conditions to obtain the full picture. In Fig. 1(a), we assume $\mu = 10^{-4}$ and plot the time average of $x_i$,

$$\bar{x}_i \equiv \frac{1}{t_2 - t_1} \int_{t_1}^{t_2} x_i(t)dt, \quad (4)$$

which removes transient dynamics for $0 \leqslant t < t_1$ with $t_1 \gg O(1)$ and considers the history up to $t_2 > t_1$. For each value of $c$, we have checked roughly $2 \times 10^4$ different initial conditions for $\mathbf{x} = (x_{\text{AllD}}, x_{\text{TFT}}, x_{\text{WSLS}})$ in $\mathcal{I}_\delta \equiv \{(0,0,0), (0,0,\delta), (0,0,2\delta), \ldots, (1,0,0)\}$ with $\delta = \frac{1}{48}$. If we take $c = 0.2$, for example, we find from Fig. 1(a) that the system has two different attractors, characterized by $\mathbf{x}^* \approx (1,0,0)$ and $\mathbf{x}^* \approx (0,0,1)$, respectively, depending on the initial condition. The latter fixed point (FP) disappears as $c$ roughly exceeds $\frac{1}{2}$, and this is readily explained by the FP analysis: when $\mu = 0$, Eq. (3) has 11 different FP's, one of which is $\mathbf{x}_0^* = (0,0,1)$. Its eigenvalues are all negative when $c$ lies below a certain threshold $c_{\text{th}} = \frac{(1-2\epsilon)^2}{2-4\epsilon+4\epsilon^2} \approx \frac{1}{2} - \epsilon$, whereas one of them becomes positive for $c > c_{\text{th}}$ (see Appendix B for details). In terms of evolutionary biology, we can also say that the WSLS-dominant FP is an evolutionarily stable state (ESS) for $c < c_{\text{th}}$, noting that an ESS constitutes an asymptotically stable FP in RD [15]. Figure 1(a) also shows that the distribution of attractors changes qualitatively as $c$ increases. Roughly speaking, if $c \gtrsim 0.4$, we can observe another attractor whose time average is approximated as $\bar{\mathbf{x}} = (\bar{x}_{\text{AllD}}, \bar{x}_{\text{TFT}}, \bar{x}_{\text{WSLS}}) \approx (\frac{1-c}{2}, c, \eta)$ with a
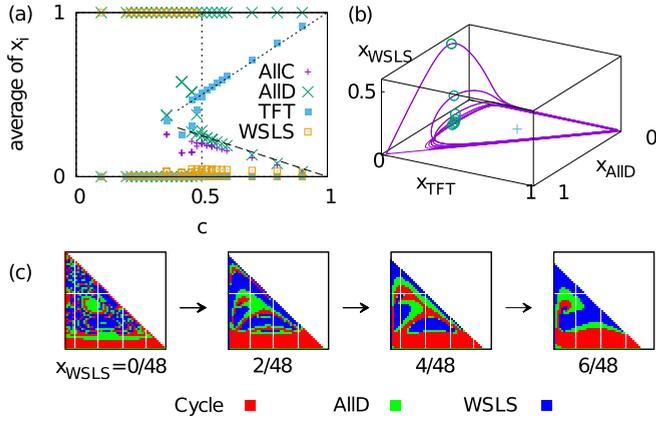
FIG. 1. (a) Fractions of strategies averaged over long time [Eq. (4)], started from various initial conditions (see the main text). The vertical dotted line indicates $c = \frac{1}{2}$, and the two oblique dotted lines represent $x_{\text{TFT}} \approx c$ and $x_{\text{AllD}} \approx \frac{1-c}{2}$, respectively. (b) Attractor for $c = 0.46$ as a stable limit cycle, which rotates counterclockwise if projected onto the $(x_{\text{TFT}}, x_{\text{AllD}})$ plane. The small circles represent local maxima of $x_{\text{WSLS}}$ along the trajectory, and the cross indicates a mutation-free fixed point (FP) written as $\mathbf{x}_0^* = (\frac{1-2\epsilon-c}{2-4\epsilon}, \frac{c}{1-2\epsilon}, 0)$. (c) Basins of attraction for $c = 0.46$, where the horizontal and vertical coordinates indicate $x_{\text{AllD}}$ and $x_{\text{TFT}}$, respectively. These are cross-sectional views at different values of $x_{\text{WSLS}}$ from $\frac{0}{48}$ to $\frac{6}{48}$. The basin of attraction for a cycle as shown in (b) is denoted in red, AllD FP with $\mathbf{x}^* = (1,0,0)$ in green, and WSLS FP with $\mathbf{x}^* = (0,0,1)$ in blue.

small positive number $\eta$. This attractor actually corresponds to a cycle, and Fig. 1(b) shows an example for $c = 0.46$. By a cycle, we do not only mean an ordinary limit cycle of finite periodicity but also a quasiperiodic or strange attractor of an infinite period. Figure 1(c) provides tomographic views of the basins of attraction with different values of $x_{\text{WSLS}}(t = 0)$. The basins have very complicated boundaries on the $(x_{\text{AllD}}, x_{\text{TFT}})$ plane and gradually merge as we increase $x_{\text{WSLS}}$ in the initial condition. Therefore, although WSLS can stabilize cooperation for $c < c_{\text{th}}$, it depends on initial conditions, and one cannot easily choose a correct one if beginning with low $x_{\text{WSLS}}$.

The complicated geometry of the basins of attraction suggests the possibility of chaos [17]. To quantify chaoticity, we calculate Lyapunov exponents with LyapOde4 [18], which is based on the QR decomposition method [19]. In Fig. 2(a), we plot the largest Lyapunov exponent $\lambda_1$ when it is estimated as positive (see Appendix C for details). The result supports the existence of chaos. Furthermore, we can explicitly construct a bifurcation diagram [Fig. 2(a)] by plotting local maxima of $x_{\text{WSLS}}$ [the circles in Fig. 1(b)] at various values of $c$. The bifurcation structure is reminiscent of that of the logistic map, and the similarity can be made more precise by plotting a return map between the $n$th and $(n + 1)$th maxima when the system is chaotic [inset of Fig. 2(a)]. We also note that Fig. 2(a) shows many other lines than the bifurcation diagram because two different cycles can coexist at the same $c$ depending on their initial conditions. For example, the upper panel of Fig. 2(b) depicts two time series of $x_{\text{WSLS}}$ at $c = 0.475$: the solid line shows two alternating peaks, whereas the dashed
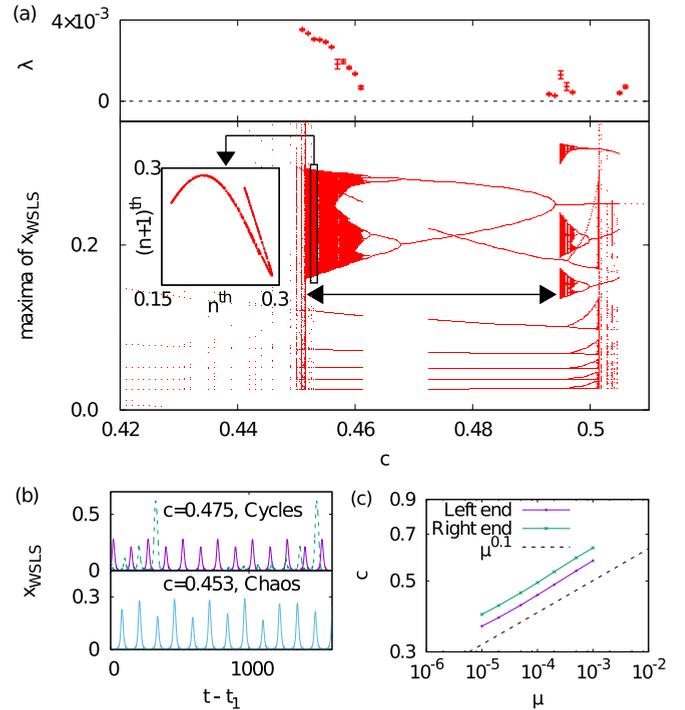


FIG. 2. (a) Largest Lyapunov exponent $\lambda_1$ when it is positive, and local maxima of $x_{\text{WSLS}}(t)$ [see the circles in Fig. 1(b)] at various values of $c$. We check many different cycles to estimate the average and standard error of $\lambda_1$. The big horizontal arrow shows the size of the main bifurcation structure, and the long vertical rectangle indicates $c = 0.453$, at which chaos fully develops. Inset: return map between the $n$th and $(n + 1)$th maxima of $x_{\text{WSLS}}$ at $c = 0.453$. (b) Time series of $x_{\text{WSLS}}$ at $c = 0.475$ (upper) and $c = 0.453$ (lower), after removing transient dynamics for $t_1 \gg O(1)$. The two lines of the upper panel are obtained with different initial conditions. (c) Left and right ends of the main bifurcation structure [see the horizontal arrow in (a)] as a function of $\mu$ on the log-log scale. We have additionally plotted $\mu^{0.1}$ for comparison.

line is characterized by gradually growing peaks followed by a quiet stage. As $c$ decreases, the former cycle undergoes period doubling to chaos [the lower panel in Fig. 2(b)], but the latter one still remains stable with finite periodicity. Although unpredictable, the dynamics exhibits a variety of correlations that we can make use of. For example, the maximum of $x_{\text{WSLS}}$ provides a precursor for that of $x_{\text{AllD}}$ because it is correlated with how close the trajectory gets to the state of $x_{\text{AllD}} = 1$ before turning toward the state of $x_{\text{TFT}} = 1$ [see Fig. 1(b)].

The position of the main bifurcation structure is extremely sensitive to the variation of $\mu$: Fig. 2(c) shows the left and right ends of the main bifurcation structure, represented by the horizontal arrow in Fig. 2(a). According to our numerical observation, they are roughly proportional to $\mu^{0.1}$. If the power-law behavior holds for $\mu \to 0$, the bifurcation structure will shrink and eventually disappear as mutation occurs less and less frequently. The exponent is unexpectedly small, and this sensitivity to $\mu$ is consistent with the following observation: Suppose that we have a FP $\mathbf{x}_0^*$ when mutation is absent, i.e., $\mu = 0$. The corresponding FP $\mathbf{x}^*$ in the presence of small $\mu > 0$ cannot be obtained directly but approximated through a perturbative calculation [20]. By denoting

$\mathbf{f}(\mathbf{x}) \equiv (f_{\text{AllD}}(\mathbf{x}), f_{\text{TFT}}(\mathbf{x}), f_{\text{WSLS}}(\mathbf{x}))$, we obtain

$$\mathbf{x}^* \approx \mathbf{x}_0^* - \mathbf{J}(\mathbf{x}_0^*)^{-1} \cdot \mathbf{f}(\mathbf{x}_0^*), \qquad (5)$$

if the Jacobian matrix $\mathbf{J} = \{\frac{\partial f_i}{\partial x_j}\}$ has an inverse at $\mathbf{x} = \mathbf{x}_0^*$ (see Appendix D for details). The last term on the right-hand side of Eq. (5) describes displacement of the FP due to mutation and it is expected to be of an order of $\mu$ in this perturbative approach. However, this is not the case if we look at a mutation-free FP $\mathbf{x}_0^* = (\frac{1-2\epsilon-c}{2-4\epsilon}, \frac{c}{1-2\epsilon}, 0)$, which is close to $\bar{\mathbf{x}} \approx (\frac{1-c}{2}, c, \eta)$, the time average of the cycle in Fig. 1(b): We rather find that $\frac{\partial f_{\text{WSLS}}}{\partial x_i}$ is only of an order of $\mu$ for every $i \in \mathcal{S}$, so that the naive perturbative analysis of Eq. (5) yields displacement of $O(1)$. Note that it does not vanish in the limit of $\mu \to 0$, contrary to our expectation. The failure in the perturbative estimate of $\mathbf{x}^*$ nevertheless suggests that mutation can greatly affect the FP structure near the limit cycle.

## IV. DISCUSSION

Whenever an ESS exists, it is an asymptotically stable FP in the mutation-free RD, i.e., Eq. (3) with $\mu = 0$, and a local Lyapunov function can be constructed in the vicinity of this FP [15,16]. However, RD may have different types of attractors such as a limit cycle and a strange attractor, and we then have no systematic way to regard the dynamic evolution as optimization of a certain target function. In this context, it is worth noting that RD has emergent symmetry [20]: Let us denote

$$dx_{\text{AllC}}/dt \equiv f_{\text{AllC}}(x_{\text{AllC}}, x_{\text{AllD}}), \qquad (6)$$

$$dx_{\text{AllD}}/dt \equiv f_{\text{AllD}}(x_{\text{AllC}}, x_{\text{AllD}}) \qquad (7)$$

with setting $x_{\text{WSLS}} = \mu = 0$. Then, the following equality holds:

$$f_{\text{AllC}}(x_{\text{AllC}}, x_{\text{AllD}}) + f_{\text{AllD}}(x_{\text{AllD}}, x_{\text{AllC}}) = 0. \qquad (8)$$

Therefore, if we redefine $X_{\text{AllC}} \equiv x_{\text{AllD}}$, $X_{\text{AllD}} \equiv x_{\text{AllC}}$, and $\tau \equiv -t$, we find from Eq. (8) that

$$dX_{\text{AllC}}/d\tau = f_{\text{AllC}}(X_{\text{AllC}}, X_{\text{AllD}}), \qquad (9)$$

$$dX_{\text{AllD}}/d\tau = f_{\text{AllD}}(X_{\text{AllC}}, X_{\text{AllD}}), \qquad (10)$$

recovering the original dynamics in Eqs. (6) and (7) (see Appendix E for more detailed derivation). In other words, if both $x_{\text{WSLS}}$ and $\mu$ are strictly zero, the dynamics is dual to itself under time reversal and exchange between AllC and AllD. The duality implies that our two-dimensional dynamics cannot have a global Lyapunov function: If a function $V(x_{\text{AllC}} = x_1, x_{\text{AllD}} = x_2)$ has a positive time derivative, $V(x_2, x_1)$ must be a decreasing function of time. Loosely speaking, therefore, if WSLS was absent, it would be impossible to define the arrow of time for the whole system based solely on selection. We have two ways for directionality at this point: One is to incorporate $x_{\text{WSLS}} > 0$ into dynamics to let the system converge to the corresponding ESS through *selection*. The other is to keep $x_{\text{WSLS}}$ at zero but introduce $\mu > 0$ and redefine the arrow of time in terms of *mutation*. For example, the FP $\mathbf{x}^*$, modified from $\mathbf{x}_0^* = (\frac{1-2\epsilon-c}{2-4\epsilon}, \frac{c}{1-2\epsilon}, 0)$ by mutation, has eigenvalues with a negative real part proportional to $\mu$ [20]. It implies that mutation mixes up the populations of different strategies so that the system

always ends up with the same polymorphic state. In either case, the initial condition eventually becomes irrelevant. Our finding implies that if both $x_{\text{WSLS}}$ and $\mu$ are turned on, the symmetry under time reversal and AllC-AllD exchange can break in a more nontrivial way. In particular, we have seen that mutation, induced by the inherent microscopic randomness of the environment, produces unpredictability on evolutionary scales. One might say that this is not unexpected because mutation *per se* is a random event which makes the evolutionary path deviate from the one determined by the initial condition. However, we are dealing with mutation in a fully deterministic manner in Eq. (3), and the effect of mutation is not just small perturbation added to a deterministic path, but the FP structure itself seems to experience nonperturbative changes. The chaotic dynamics is directional in a rather subtle sense that the path reveals more and more information of the initial condition as time goes by. Differently from the above cases, this additional information is not a function of the current state exclusively, but something evaluated with reference to history [21]. Historical contingency should be understood in this respect, considering that not all history-dependent systems are chaotic.

## V. SUMMARY

In summary, we have presented numerical evidence that chaos exists in the 3D continuous-time RD with mutation among the four representative strategies of the PD game, i.e., AllC, AllD, TFT, and WSLS. Even if one considers a more general strategy space, it will contain these four in most cases, and our findings will remain valid in the corresponding subspace. The model, originally motivated by selection against the better for the population, provides a simple analytic picture for nonprogressionism, showing various facets of mutation: it generates unpredictability with exerting nonperturbative effects on evolutionary paths and breaks symmetry of a subsystem under time reversal. The strategic interaction considered here is one of the most intensively studied subjects in evolutionary game theory, so our finding suggests that chaos can be more prevalent than previously known.

## APPENDIX A: DERIVATION OF LONG-TERM PAYOFF $a_{ij}$

As mentioned in the main text, we denote by $q_{\alpha\beta}$ ($r_{\beta\alpha}$) the probability that the player (coplayer) with strategy $i$ ($j$) cooperates at the next round, given that the state of player's and coplayer's moves is $(\alpha, \beta)$ at the current round. Here, $\alpha, \beta \in$

$\{C,D\}$. We summarize the values of $q_{\alpha\beta}$ for each strategy $i \in \mathcal{S} = \{\text{AllC, AllD, TFT, WSLS}\}$ as follows:

| $(\alpha,\beta)$ | AllC | AllD | TFT | WSLS |
|---|---|---|---|---|
| $(C,C)$ | 1 | 0 | 1 | 1 |
| $(C,D)$ | 1 | 0 | 0 | 0 |
| $(D,C)$ | 1 | 0 | 1 | 0 |
| $(D,D)$ | 1 | 0 | 0 | 1 |

The values of $r_{\beta\alpha}$ for the coplayer with strategy $j$ can be similarly assigned.

In the presence of implementation error with probability $\epsilon \in (0,1)$, the probabilities of cooperating are effectively changed to $q'_{\alpha\beta} = (1-\epsilon)q_{\alpha\beta} + \epsilon(1-q_{\alpha\beta})$ and $r'_{\beta\alpha} = (1-\epsilon) r_{\beta\alpha} + \epsilon(1-r_{\beta\alpha})$, respectively. By defining $\bar{q}'_{\alpha\beta} \equiv 1 - q'_{\alpha\beta}$ and $\bar{r}'_{\beta\alpha} \equiv 1 - r'_{\beta\alpha}$, the transition matrix between the current and next states is written as

$$M = \begin{bmatrix} q'_{CC}r'_{CC} & q'_{CD}r'_{DC} & q'_{DC}r'_{CD} & q'_{DD}r'_{DD} \\ q'_{CC}\bar{r}'_{CC} & q'_{CD}\bar{r}'_{DC} & q'_{DC}\bar{r}'_{CD} & q'_{DD}\bar{r}'_{DD} \\ \bar{q}'_{CC}r'_{CC} & \bar{q}'_{CD}r'_{DC} & \bar{q}'_{DC}r'_{CD} & \bar{q}'_{DD}r'_{DD} \\ \bar{q}'_{CC}\bar{r}'_{CC} & \bar{q}'_{CD}\bar{r}'_{DC} & \bar{q}'_{DC}\bar{r}'_{CD} & \bar{q}'_{DD}\bar{r}'_{DD} \end{bmatrix}. \quad (A1)$$

Then, from the equation of $M\vec{v} = \vec{v}$, we obtain the stationary solution as $\vec{v} = (v_{CC}, v_{CD}, v_{DC}, v_{DD})$, which is a unique right eigenvector of the matrix $M$. Here, we impose the normalization for $\vec{v}$ using $v_{CC} + v_{CD} + v_{DC} + v_{DD} = 1$. Then, $v_{\alpha\beta}$ can be interpreted as the stationary probability of finding the state $(\alpha,\beta)$ when players with strategies $i$ and $j$ play the game. The results of $\vec{v}$ for all combinations of $i$ and $j$ are summarized in Table I. Once $\vec{v}$ is obtained, we calculate the long-term payoff $a_{ij}$ that the strategy $i$ obtains against $j$, by taking the inner product between $\vec{v}$ and the payoff vector such that

$$a_{ij} = \vec{v} \cdot (b-c, -c, b, 0). \quad (A2)$$

The long-term payoffs $a_{ij}$ for all possible pairs of $i$ and $j$ are presented in Table II. Note that with $\epsilon > 0$, initial states are irrelevant in the long run.

## APPENDIX B: FP ANALYSIS OF THE REPLICATOR DYNAMICS WHEN $\mu = 0$

In order to better understand the RD in Eq. (3) in the main text, we first analyze the mutation-free case, i.e., when $\mu = 0$. Let us define $\mathbf{x} \equiv (x_{\text{AllD}}, x_{\text{TFT}}, x_{\text{WSLS}})$, where $x_i$ denotes the fraction of strategy $i$. From the set of equations

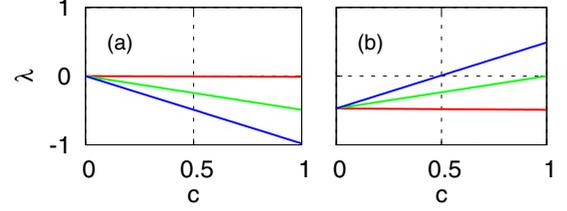$$0 = \frac{dx_i}{dt} = f_i(\mu = 0) = p_i x_i - \langle p \rangle x_i \quad (B1)$$



FIG. 3. (a) Eigenvalues for the first FP of Eq. (B2), $\mathbf{x}_0^* = (x_{\text{AllD}}^*, x_{\text{TFT}}^*, x_{\text{WSLS}}^*) = (1,0,0)$. All of the eigenvalues are negative for the entire range of $c$. We set $b = 1$ without loss of generality and choose $\epsilon = 10^{-2}$. (b) Eigenvalues for another FP $(0,0,1)$. The largest eigenvalue is negative for $c < c_{\text{th}}$. The threshold value $c_{\text{th}}$ is analytically obtained in Eq. (B4).

for all $i \in \mathcal{S}$, we analytically find 11 different FP's $\mathbf{x}_0^*$ as follows:

$$\mathbf{x}_0^* = \begin{cases} (1,0,0), \\ (0,1,0), \\ (0,0,1), \\ (0,0,0), \\ \left(0,0,-\frac{c}{(1-2\epsilon)^2(b-c)}\right), \\ \left(0,\frac{2c\epsilon}{(b-c)(1-2\epsilon)},0\right), \\ \left(\frac{b(1-2\epsilon)-c}{2b(1-2\epsilon)},\frac{c}{b(1-2\epsilon)},0\right), \\ \left(\frac{b(1-2\epsilon)-c}{(b-c)(1-2\epsilon)},\frac{2c\epsilon}{(b-c)(1-2\epsilon)},0\right), \\ \left(\frac{(b-c)(1-2\epsilon)^2-c}{(b-c)(1-2\epsilon)^2},0,\frac{c}{(b-c)(1-2\epsilon)^2}\right), \\ \left(0,\frac{c[2(b-c)\epsilon(1-2\epsilon)-c]}{(1-2\epsilon)[(b-c)^2(1-2\epsilon)-bc]},\frac{c[b(2\epsilon-1)+c]}{(1-2\epsilon)[(b-c)^2(1-2\epsilon)+bc]}\right), \\ \left(\frac{(b-c)[b(1-2\epsilon)-c]}{(b-c)^2(1-2\epsilon)+bc},\frac{c[2(b-c)\epsilon(1-2\epsilon)+c]}{(1-2\epsilon)[(b-c)^2(1-2\epsilon)+bc]},\right. \\ \left.\frac{c[b(1-2\epsilon)-c]}{(1-2\epsilon)[(b-c)^2(1-2\epsilon)-bc]}\right). \end{cases}$$
$$(B2)$$

By the linear stability analysis, we find that only one FP $\mathbf{x}_0^* = (1,0,0)$, implying $x_{\text{AllD}} = 1$, is stable for the entire range of $c$, confirmed by the negativity of all eigenvalues, as shown in Fig. 3(a). This result is somehow consistent with the fact that this FP is numerically observed for the entire range of $c$ even when $\mu > 0$, as depicted in Fig. 1(a) in the main text. We are also interested in another FP $\mathbf{x}_0^* = (0,0,1)$, i.e., $x_{\text{WSLS}} = 1$. It is found that the largest eigenvalue is negative for $c < c_{\text{th}}$ with some threshold $c_{\text{th}}$, implying that the FP is stable. However, it becomes positive for $c > c_{\text{th}}$, implying instability of the FP. See Fig. 3(b). This largest eigenvalue is calculated as

$$\lambda = \left(\epsilon - \frac{1}{2}\right)\{b(1-2\epsilon)^2 - 2c[2(\epsilon-1)\epsilon+1]\}, \quad (B3)$$

from which we can define $c_{\text{th}}$ as follows:

$$c_{\text{th}} = \frac{b(1-2\epsilon)^2}{2(1-2\epsilon+2\epsilon^2)} \approx b\left(\frac{1}{2}-\epsilon\right). \quad (B4)$$

All the other FP's turn out to be unstable.

## APPENDIX C: POSITIVE LYAPUNOV EXPONENTS

For chaotic dynamics, the largest Lyapunov exponent is positive. The problem arises when its value is so small that

TABLE I. Stationary probability distributions $v_{\alpha\beta}$ of finding the state $(\alpha,\beta)$ when strategy $i$ plays against $j$, where $(\alpha,\beta)$ can be one of the four states: $(C,C)$, $(C,D)$, $(D,C)$, and $(D,D)$.

| $i$ | $j$ | $v_{CC}$ | $v_{CD}$ | $v_{DC}$ | $v_{DD}$ |
|---|---|---|---|---|---|
| AllC | AllC | $(1-\epsilon)^2$ | $\epsilon(1-\epsilon)$ | $\epsilon(1-\epsilon)$ | $\epsilon^2$ |
| | AllD | $\epsilon(1-\epsilon)$ | $(1-\epsilon)^2$ | $\epsilon^2$ | $\epsilon(1-\epsilon)$ |
| | TFT | $1-3\epsilon+4\epsilon^2-2\epsilon^3$ | $2\epsilon(1-\epsilon)^2$ | $\epsilon(1-2\epsilon-2\epsilon^2)$ | $2\epsilon^2(1-\epsilon)$ |
| | WSLS | $(1-\epsilon)/2$ | $(1-\epsilon)/2$ | $\epsilon/2$ | $\epsilon/2$ |
| AllD | AllC | $\epsilon(1-\epsilon)$ | $\epsilon^2$ | $(1-\epsilon)^2$ | $\epsilon(1-\epsilon)$ |
| | AllD | $\epsilon^2$ | $\epsilon(1-\epsilon)$ | $\epsilon(1-\epsilon)$ | $(1-\epsilon)^2$ |
| | TFT | $2\epsilon^2(1-\epsilon)$ | $\epsilon(1-2\epsilon-2\epsilon^2)$ | $2\epsilon(1-\epsilon)^2$ | $1-3\epsilon+4\epsilon^2-2\epsilon^3$ |
| | WSLS | $\epsilon/2$ | $\epsilon/2$ | $(1-\epsilon)/2$ | $(1-\epsilon)/2$ |
| TFT | AllC | $1-3\epsilon+4\epsilon^2-2\epsilon^3$ | $\epsilon(1-2\epsilon+2\epsilon^2)$ | $2\epsilon(1-\epsilon)^2$ | $2\epsilon^2(1-\epsilon)$ |
| | AllD | $2\epsilon^2(1-\epsilon)$ | $2\epsilon(1-\epsilon)^2$ | $\epsilon(1-2\epsilon+2\epsilon^2)$ | $1-3\epsilon+4\epsilon^2-2\epsilon^3$ |
| | TFT | $1/4$ | $1/4$ | $1/4$ | $1/4$ |
| | WSLS | $1/4$ | $1/4$ | $1/4$ | $1/4$ |
| WSLS | AllC | $(1-\epsilon)/2$ | $\epsilon/2$ | $(1-\epsilon)/2$ | $\epsilon/2$ |
| | AllD | $\epsilon/2$ | $(1-\epsilon)/2$ | $\epsilon/2$ | $(1-\epsilon)/2$ |
| | TFT | $1/4$ | $1/4$ | $1/4$ | $1/4$ |
| | WSLS | $1-4\epsilon+7\epsilon^2-4\epsilon^3$ | $\epsilon(1-\epsilon)$ | $\epsilon(1-\epsilon)$ | $\epsilon(2-5\epsilon+4\epsilon^2)$ |

the numerical error of the algorithm has the same order of magnitude. Suppose that we have a continuous orbit in a bounded three-dimensional region and its Lyapunov exponents are sorted in descending order, i.e., $\lambda_1 > \lambda_2 > \lambda_3$. It is well known that one of the Lyapunov exponents must be zero for a continuous orbit. We can also be sure that $\lambda_3$ must be negative for the following reason: the information dimension of an attractor is bounded from above by the Kaplan-Yorke formula

$$D_{\mathrm{KY}} = j + \frac{\sum_{i=1}^{j}\lambda_i}{|\lambda_{j+1}|}, \quad \text{(C1)}$$

where $j$ satisfies $\sum_{i=1}^{j}\lambda_i > 0$ and $\sum_{i=1}^{j+1}\lambda_i < 0$. In our case, the dimension cannot be greater than three, which means that $j \leqslant 2$. From $\sum_{i=1}^{3}\lambda_i < 0$, it follows that $\lambda_3 < 0$.

Based on these results, we draw the following conclusions: if we have a chaotic orbit, it implies that $\lambda_1 > 0$ whereas $\lambda_2$ is zero. Therefore, we have the following inequality:

$$\lambda_1 + \lambda_2 > 0. \quad \text{(C2)}$$

On the other hand, if $\lambda_1$ is actually zero but numerically estimated as a tiny positive number, $\lambda_1 + \lambda_2$ is likely to be negative because of $\lambda_2$. The point is that Eq. (C2) provides a sharp criterion to check the positivity of $\lambda_1$, which can sometimes be obscure if we observe $\lambda_1$ only. The Lyapunov

exponents depicted in Fig. 1 of the main text are estimated as positive in this way.

### APPENDIX D: PERTURBATIVE ANALYSIS FOR SMALL POSITIVE $\mu$

Based on the understanding of the mutation-free case in Appendix B, we now analyze a more general case with $\mu > 0$. As it is not straightforward to obtain the FP's of the RD in Eq. (3) in the main text, we take the perturbative approach. More specifically, we apply Newton's method in which each FP $\mathbf{x}_0^*$ for $\mu = 0$ serves as a trial solution. The first order Taylor expansion around the FP $\mathbf{x}_0^* = (x_{0,\mathrm{AllD}}^*, x_{0,\mathrm{TFT}}^*, x_{0,\mathrm{WSLS}}^*)$ yields the following equation:

$$\mathbf{0} = \begin{pmatrix} f_{\mathrm{AllD}}(\mathbf{x}^*) \\ f_{\mathrm{TFT}}(\mathbf{x}^*) \\ f_{\mathrm{WSLS}}(\mathbf{x}^*) \end{pmatrix} = \begin{pmatrix} f_{\mathrm{AllD}}(\mathbf{x}_0^*) \\ f_{\mathrm{TFT}}(\mathbf{x}_0^*) \\ f_{\mathrm{WSLS}}(\mathbf{x}_0^*) \end{pmatrix}$$

$$+ \begin{pmatrix} \frac{\partial f_{\mathrm{AllD}}}{\partial x_{\mathrm{AllD}}} & \frac{\partial f_{\mathrm{AllD}}}{\partial x_{\mathrm{TFT}}} & \frac{\partial f_{\mathrm{AllD}}}{\partial x_{\mathrm{WSLS}}} \\ \frac{\partial f_{\mathrm{TFT}}}{\partial x_{\mathrm{AllD}}} & \frac{\partial f_{\mathrm{TFT}}}{\partial x_{\mathrm{TFT}}} & \frac{\partial f_{\mathrm{TFT}}}{\partial x_{\mathrm{WSLS}}} \\ \frac{\partial f_{\mathrm{WSLS}}}{\partial x_{\mathrm{AllD}}} & \frac{\partial f_{\mathrm{WSLS}}}{\partial x_{\mathrm{TFT}}} & \frac{\partial f_{\mathrm{WSLS}}}{\partial x_{\mathrm{WSLS}}} \end{pmatrix} \begin{pmatrix} x_{\mathrm{AllD}}^* - x_{0,\mathrm{AllD}}^* \\ x_{\mathrm{TFT}}^* - x_{0,\mathrm{TFT}}^* \\ x_{\mathrm{WSLS}}^* - x_{0,\mathrm{WSLS}}^* \end{pmatrix}, \quad \text{(D1)}$$

where $\mathbf{x}^* = (x_{\mathrm{AllD}}^*, x_{\mathrm{TFT}}^*, x_{\mathrm{WSLS}}^*)$ denotes the corresponding perturbative solution. The matrix in the above equation is indeed

TABLE II. Long-term payoff $a_{ij}$ that strategy $i$ (leftmost column) obtains against $j$ (top row).

| | AllC | AllD | TFT | WSLS |
|---|---|---|---|---|
| AllC | $(b-c)(1-\epsilon)$ | $b\epsilon - c(1-\epsilon)$ | $b(1-2\epsilon+2\epsilon^2) - c(1-\epsilon)$ | $\frac{b}{2} - c(1-\epsilon)$ |
| AllD | $b(1-\epsilon) - c\epsilon$ | $(b-c)\epsilon$ | $[2b(1-\epsilon)-c]\epsilon$ | $\frac{1}{2}(b-2c\epsilon)$ |
| TFT | $b(1-\epsilon) - c(1-2\epsilon-2\epsilon^2)$ | $[b-2c(1-\epsilon)]\epsilon$ | $\frac{b-c}{2}$ | $\frac{b-c}{2}$ |
| WSLS | $b(1-\epsilon) - \frac{c}{2}$ | $b\epsilon - \frac{c}{2}$ | $\frac{b-c}{2}$ | $(b-c)(1-3\epsilon+6\epsilon^2-4\epsilon^3)$ |

Jacobian matrix $\mathbf{J} = \{\frac{\partial f_i}{\partial x_j}\}$ calculated at $\mathbf{x} = \mathbf{x}_0^*$. If $\mathbf{J}(\mathbf{x}_0^*)$ has an inverse, by arranging Eq. (D1), we get

$$\begin{pmatrix} x_{\text{AllD}}^* \\ x_{\text{TFT}}^* \\ x_{\text{WSLS}}^* \end{pmatrix} \approx \begin{pmatrix} x_{0,\text{AllD}}^* \\ x_{0,\text{TFT}}^* \\ x_{0,\text{WSLS}}^* \end{pmatrix} - \mathbf{J}^{-1} \begin{pmatrix} f_{\text{AllD}}(\mathbf{x}_0^*) \\ f_{\text{TFT}}(\mathbf{x}_0^*) \\ f_{\text{WSLS}}(\mathbf{x}_0^*) \end{pmatrix}. \qquad \text{(D2)}$$

Here, we would like to note that even when $\mathbf{J}(\mathbf{x}_0^*)$ has no inverse, one can first calculate $\mathbf{J}(\mathbf{x})^{-1}$, then substitute $\mathbf{x}$ by

$\mathbf{x}_0^*$ to obtain the result $\mathbf{x}^*$ in Eq. (5b). Then, based on numerical observations, we pick up three FP's for $\mu = 0$, i.e., $(1,0,0)$, $(0,0,1)$, and $(\frac{b(1-2\epsilon)-c}{2b(1-2\epsilon)}, \frac{c}{b(1-2\epsilon)}, 0)$. For example, the last one is chosen because it behaves similarly to $\bar{\mathbf{x}} \approx (\frac{1-c}{2}, c, \eta)$ with small positive $\eta$, when the time average is taken over the cycle (see the main text). We will denote this last FP as $\hat{\mathbf{x}}_0^*$. By applying Newton's method to these FP's, we obtain the following perturbative solutions:

$$\mathbf{x}^* \approx \begin{cases} \begin{pmatrix} 1 \\ 0 \\ 0 \end{pmatrix} & +\mu \begin{pmatrix} \frac{(3\epsilon+1)(b-c)}{3c-6c\epsilon} \\ -\frac{(b-c)}{3c-6c\epsilon} \\ \frac{2\epsilon(b-c)}{3c(2\epsilon-1)} \end{pmatrix}, \\[20pt] \begin{pmatrix} 0 \\ 0 \\ 1 \end{pmatrix} & +\mu \begin{pmatrix} -\frac{2[(\epsilon-1)(4\epsilon^2-2\epsilon+1)(b-c)]}{3((2\epsilon-1)\{b(1-2\epsilon)^2-2c[2(\epsilon-1)\epsilon+1]\})} \\ \frac{1}{3}\left(\frac{1}{(2\epsilon-1)^3}-1\right) \\ \frac{2(\epsilon-1)(4\epsilon^2-2\epsilon+1)(3b^2(1-2\epsilon)^4-6bc(1-2\epsilon)^4+2c^2\{12(\epsilon-1)\epsilon[2(\epsilon-1)\epsilon+1]+1\})}{3(2\epsilon-1)^3[b(1-2\epsilon)^2-4c(\epsilon-1)\epsilon]\{b(1-2\epsilon)^2-2c[2(\epsilon-1)\epsilon+1]\}} \end{pmatrix}, \\[28pt] \begin{pmatrix} \frac{b(1-2\epsilon)-c}{2b(1-2\epsilon)} \\ \frac{c}{b(1-2\epsilon)} \\ 0 \end{pmatrix} & +\mu \begin{pmatrix} \frac{(b-c)[2\epsilon(b+c)-5b-c][b(2\epsilon-1)+4c]}{24c^2(2\epsilon-1)[b(2\epsilon-1)+c]} \\ 0 \\ -\frac{\{(b-c)(b+c)[b(2\epsilon-1)+4c]\}}{12\{c^2[b(2\epsilon-1)+c]\}} \end{pmatrix} + \begin{pmatrix} \frac{1}{8} \\ 0 \\ -\frac{1}{4} \end{pmatrix}. \end{cases} \qquad \text{(D3)}$$

We find that a term of $O(1)$ appears for $\hat{\mathbf{x}}_0^*$ because of $\mu \ll 1$, implying that the perturbative approach fails here. The result can be understood by directly calculating $\mathbf{J}(\mathbf{x}_0^*)$ for $\mu \to 0$:

$$\mathbf{J}\left(\frac{b(1-2\epsilon)-c}{2b(1-2\epsilon)}, \frac{c}{b(1-2\epsilon)}, 0\right)$$
$$= \frac{[c-b(1-2\epsilon)]}{4b^2} \begin{pmatrix} 2c^2 & c^2+b^2(1-2\epsilon) & c^2 \\ -4c^2 & -2c^2 & -2c^2 \\ 0 & 0 & 0 \end{pmatrix}. \qquad \text{(D4)}$$

This Jacobian matrix has zeros in the bottom row because $\nabla f_{\text{WSLS}} \to 0$ in the limit of zero mutation. In fact, one can readily check that $f_{\text{WSLS}}$ becomes a constant function in this limit for every $\mathbf{x}$ such that $x_{\text{TFT}} = 1 - 2x_{\text{AllD}}$ and $x_{\text{WSLS}} = 0$. The FP $\hat{\mathbf{x}}_0^*$ also satisfies this condition, so every derivative vanishes there along the direction of $(1, -2, 0)$. As a consequence, even if we include higher-order derivatives in the Taylor expansion [Eq. (D1)], the resulting matrices will always be singular. For example, the Hessian matrix $\mathbf{H} \equiv \{\frac{\partial^2 f_{\text{WSLS}}}{\partial x_i \partial x_j}\}$ for the second-derivative test is obtained as

$$\mathbf{H}(\hat{\mathbf{x}}_0^*) = \begin{pmatrix} 0 & 0 & \frac{c^2(-1+2\epsilon)}{b} \\ 0 & 0 & \frac{c^2(-1+2\epsilon)}{b} \\ \frac{c^2(-1+2\epsilon)}{b} & \frac{c^2(-1+2\epsilon)}{2b} & \frac{c^2-b^2(1-2\epsilon)^2-bc(1-2\epsilon)^3}{b} \end{pmatrix} \qquad \text{(D5)}$$

when $\mu \to 0$. It is straightforward to see that it has an eigenvector $(1, -2, 0)$ associated with the eigenvalue zero, which makes the test inconclusive.

## APPENDIX E: SYMMETRY OF REPLICATOR DYNAMICS

Recall that RD in this work is defined as

$$\frac{dx_i}{dt} = f_i \equiv (1-\mu)p_i x_i - \langle p \rangle x_i + \frac{\mu}{|\mathcal{S}|-1}\sum_{j \neq i} p_j x_j, \qquad \text{(E1)}$$

where $p_i = \sum_i a_{ij} x_j$ and $\langle p \rangle \equiv \sum_i p_i x_i = \sum_{ij} a_{ij} x_i x_j$. The long-term payoff $a_{ij}$ is given in Table II. We explicitly write the functional dependence as $f_i(x_{\text{AllC}}, x_{\text{AllD}}, x_{\text{WSLS}})$ by choosing three independent variables. Note that we have just chosen $x_{\text{AllC}}$ as an independent variable instead of $x_{\text{TFT}}$ as we have done in other parts of the paper. It is because this set of independent variables show the symmetry most clearly. After some algebra, we can readily see the following equality:

$$f_{\text{AllC}}(x_1, x_2, x_3) + f_{\text{AllD}}(x_2, x_1, x_3)$$
$$= \frac{b-c}{3}(1+x_3)[\mu(1+x_3) - x_1(4\mu+3x_3)]. \qquad \text{(E2)}$$

It is important to note that $x_1$ and $x_2$ exchange the positions in evaluating $f_{\text{AllD}}$. Let us set $\mu$ and $x_3$ to zero so that the right-hand side vanishes altogether. We may suppress the dependence on $x_3$ which is fixed, so the result is

$$f_{\text{AllC}}(x_1, x_2) = -f_{\text{AllD}}(x_2, x_1). \qquad \text{(E3)}$$

By construction, we already have

$$\frac{dx_{\text{AllC}}}{dt} = f_{\text{AllC}}(x_{\text{AllC}}, x_{\text{AllD}}), \qquad \text{(E4)}$$

$$\frac{dx_{\text{AllD}}}{dt} = f_{\text{AllD}}(x_{\text{AllC}}, x_{\text{AllD}}). \qquad \text{(E5)}$$

We combine Eqs. (E3) to (E5) to obtain

$$\frac{dx_{\text{AllC}}}{dt} = -f_{\text{AllD}}(x_{\text{AllD}}, x_{\text{AllC}}),$$
(E6)

$$\frac{dx_{\text{AllD}}}{dt} = -f_{\text{AllC}}(x_{\text{AllD}}, x_{\text{AllC}}).$$
(E7)

Now, let us define $\tau \equiv -t$ to rewrite the equations as

$$\frac{dx_{\text{AllC}}}{d\tau} = f_{\text{AllD}}(x_{\text{AllD}}, x_{\text{AllC}}),$$
(E8)

$$\frac{dx_{\text{AllD}}}{d\tau} = f_{\text{AllC}}(x_{\text{AllD}}, x_{\text{AllC}}).$$
(E9)

Finally, the variables are relabeled as $X_{\text{AllC}} \equiv x_{\text{AllD}}$ and $X_{\text{AllD}} \equiv x_{\text{AllC}}$, and we end up with the following set of equations:

$$\frac{dX_{\text{AllD}}}{d\tau} = f_{\text{AllD}}(X_{\text{AllC}}, X_{\text{AllD}}),$$
(E10)

$$\frac{dX_{\text{AllC}}}{d\tau} = f_{\text{AllC}}(X_{\text{AllC}}, X_{\text{AllD}}),$$
(E11)

which are formally identical to the original ones [Eqs. (E4) and (E5)].

---

[1] S. J. Gould, *Wonderful Life* (W. W. Norton, New York, 1989).

[2] T. Shanahan, *The Evolution of Darwinism: Selection, Adaptation and Progress in Evolutionary Biology* (Cambridge University Press, Cambridge, UK, 2004).

[3] H. Matsuda and P. A. Abrams, Evolution **48**, 1764 (1994); M. Gyllenberg and K. Parvinen, Bull. Math. Biol. **63**, 981 (2001); M. Gyllenberg, K. Parvinen, and U. Dieckmann, J. Math. Biol. **45**, 79 (2002); D. J. Rankin and A. López-Sepulcre, Oikos **111**, 616 (2005).

[4] W. M. Muir and R. D. Howard, Proc. Natl. Acad. Sci. USA **96**, 13853 (1999).

[5] D. J. Rankin, K. Bargum, and H. Kokko, Trends Ecol. Evol. **22**, 643 (2007).

[6] M. Doebeli and I. Ispolatov, Evolution **68**, 1365 (2014).

[7] D. Vilone, A. Robledo, and A. Sánchez, Phys. Rev. Lett. **107**, 038101 (2011); T. Galla and J. D. Farmer, Proc. Natl. Acad. Sci. USA **110**, 1232 (2013).

[8] M. Nowak and K. Sigmund, Proc. Natl. Acad. Sci. USA **90**, 5091 (1993).

[9] B. Skyrms, J. Logic Lang. Inform. **1**, 111 (1992); S. H. Strogatz, *Nonlinear Dynamics and Chaos: With Applications to Physics, Biology, Chemistry, and Engineering* (Westview Press, Boulder, CO, 2001).

[10] M. Travisano, J. A. Mongold, A. F. Bennett, R. E. Lenski *et al.*, Science **267**, 87 (1995); Z. D. Blount, C. Z. Borland, and R. E. Lenski, Proc. Natl. Acad. Sci. USA **105**, 7899 (2008); P. Shah, D. M. McCandlish, and J. B. Plotkin, **112**, E3226 (2015).

[11] R. Axelrod, *The Evolution of Cooperation* (Basic Books, New York, 1984); M. A. Nowak and K. Sigmund, Nature (London) **355**, 250 (1992); L. A. Imhof, D. Fudenberg, and M. A. Nowak, Proc. Natl. Acad. Sci. USA **102**, 10797 (2005).

[12] D. Kraines and V. Kraines, Theory Decis. **26**, 47 (1989); M. A. Nowak and K. Sigmund, Nature (London) **364**, 56 (1993); M. Posch, J. Theor. Biol. **198**, 183 (1999); A. J. Bladon, T. Galla, and A. J. McKane, Phys. Rev. E **81**, 066122 (2010); C. Hilbe, L. A. Martinez-Vaquero, K. Chatterjee, and M. A. Nowak, Proc. Natl. Acad. Sci. USA **114**, 4715 (2017).

[13] L. A. Imhof, D. Fudenberg, and M. A. Nowak, J. Theor. Biol. **247**, 574 (2007); C. Hilbe, M. A. Nowak, and K. Sigmund, Proc. Natl. Acad. Sci. USA **110**, 6913 (2013); S. K. Baek, H.-C. Jeong, C. Hilbe, and M. A. Nowak, Sci. Rep. **6**, 25676 (2016).

[14] G. S. Wilkinson, Nature (London) **308**, 181 (1984); M. Milinski, *ibid.* **325**, 433 (1987).

[15] J. W. Weibull, *Evolutionary Game Theory* (MIT Press, Cambridge, MA, 1995).

[16] J. Hofbauer and K. Sigmund, *Evolutionary Games and Population Dynamics* (Cambridge University Press, Cambridge, UK, 1998).

[17] S. W. McDonald, C. Grebogi, E. Ott, and J. A. Yorke, Phys. D (Amsterdam) **17**, 125 (1985).

[18] P. H. Bryant, available at http://biocircuits.ucsd.edu/pbryant.

[19] J.-P. Eckmann and D. Ruelle, Rev. Mod. Phys. **57**, 617 (1985); H. D. Abarbanel, R. Brown, and M. B. Kennel, Int. J. Mod. Phys. B **5**, 1347 (1991).

[20] S. K. Baek, S. D. Yi, and H.-C. Jeong, J. Theor. Biol. **430**, 215 (2017).

[21] R. Wackerbauer, A. Witt, H. Atmanspacher, J. Kurths, and H. Scheingraber, Chaos Soliton. Fract. **4**, 133 (1994).